Marine Systems Supplement

On the Resistance of Blunt Forms

PETER R. PAYNE*
Peter R. Payne Inc., Rockville, Md.

Box-shaped hulls are used for a number of craft, of which the tracked amphibian supply or assault craft are probably the most familiar. This paper reviews briefly the resistance components of such a blunt form and then develops a theory that gives the wave drag component of the total resistance. Comparison with experiment gives good agreement.

BOX-SHAPED hulls are used for a number of craft, of which the tracked amphibian supply or assault craft[1] is probably the most familiar. This paper is concerned primarily with the calculation of the resistance of such a hull. However, to place the subject in a proper perspective we first examine the over-all performance parameters.

One way of expressing the resistance of a blunt form is to reduce it to a "drag coefficient" (C_D) based on some characteristic area of the form. Hays[2] has used the "statically immersed frontal area" (A_F) shown in Fig. 1, as well as the actual (dynamic) wetted frontal area. In the present paper we follow Hoerner[3] by employing the first of these alternatives, that is,

$$C_D = \text{resistance}/\tfrac{1}{2}\rho u^2 A_F \tag{1}$$

where ρ is the mass density of water, μ is the speed, and A_F is the statically immersed frontal area shown in Fig. 1. Now the equilibrium speed at a particular power setting is obtained when the thrust available from the propulsor is equal to the resistance, as indicated in Figure 2a. We also may express this in terms of power, since the power required is

$$P_D = \text{resistance} \times \text{speed} = Du \tag{2}$$

and the power available is

$$P_A = \eta_P\, 550(\text{BHP}) \tag{3}$$

where σ_P is the efficiency of the propulsor, defined as (thrust × speed)/(power input), and (BHP) is the input brake horsepower. This alternative presentation is shown in Fig. 2b. Equating the power required to the power available and using Eq. (1) for the resistance, we obtain

$$550\ \eta_P(\text{BHP}) = C_D\ \tfrac{1}{2}\rho u_{\max}{}^2 A_F \tag{4}$$

so that the maximum speed is

$$u_{\max} = [1100(\text{BHP})/\rho A_F]^{1/3}(\eta_P/C_D)^{1/3} \tag{5}$$

The significant parameters that govern the speed attainable are, therefore: a) the installed power per unit frontal area (BHP/A_F) and b) the ratio of the propulsive efficiency to the form drag coefficient (η_P/C_D).

For parallelepipeda it is of interest to express the statically immersed frontal area in terms of gross weight (W), using the Principle of Archimedes.

$$A_F = W/\rho lg \tag{6}$$

Substituting in Eq. (5),

$$u_{\max} = (1100g)^{1/3}[(\text{BHP})l/W]^{1/3}(\eta_P/C_D)^{1/3} \tag{7}$$

In this form the power loading parameter is now independent of the frontal area and depends only upon installed power, gross weight, and the length of the craft. For forms that are not parallelepipeda but still bluff, the above analysis can be modified by including a volume ratio factor in Eq. (6), which will then appear in the denominator of Eq. (7).

Defining a power loading parameter,

$$\Lambda = 35{,}400(\text{BHP})l/W \tag{8}$$

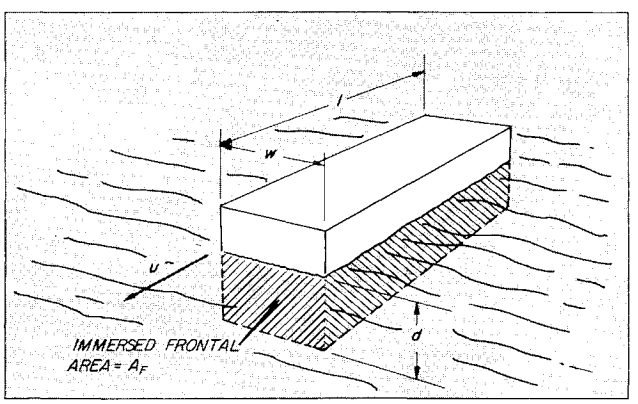

Fig. 1 Definition of blunt form geometry.

Table 1 Performance parameters for some typical track-propelled amphibians[a]

Type	W (lb)	BHP	l (ft)	$u_{\max}$ (mph)	$\Lambda^{1/2}$	η_P/C_D
LVTP5A1	81,780	810	29.7	6.8	21.8	0.0955
LVTH6	86,600	810	29.7	6.8	21.4	0.1012
LVTR1	82,200	810	31.8	6.8	22.3	0.0898
LVTE1	88,633	810	29.7	5.8	21.3	0.0642
LVTP6	50,600	430	21.6	5.5	18.7	0.0812
M-113	23,860	215	16.0	3.5	17.3	0.0261
M-29	6000	65	16.0	4.0	18.3	0.0330
M-76	12,000	127	16.7	4.5	18.4	0.0461
M-116	10,600	160	15.0	4.0	20.0	0.0253
XM-571	7700	70	19.5	2.1	18.5	0.0046
LVA-X1	6250	102	16.7	6.4	21.3	0.0859
LVT-3	35,600	220	24.5	6.0	17.5	0.1272
LVT-4	32,150	250	26.2	7.0	19.3	0.1503

[a] See Ref. 1.

Received November 8, 1965. This work was supported by the Office of Naval Research under Contract Nonr-4626(00) on behalf of the U. S. Marine Corps Exploratory Development Requirement TM 2.0.1-"Amphibian Vehicle Improvement."

* President. Member AIAA.

Eq. (7) becomes

$$u_{\max} = \Lambda^{1/3}(\eta_P/C_D)^{1/3} \tag{9}$$

The power loading parameter Λ has been evaluated for some typical track-propelled amphibious vehicles in Table 1, using data from Ref. 1.

Factor of Merit

The parameter (η_P/C_D) is a factor of merit that may be regarded as a measure of the designer's skill. An efficient propulsion system coupled with a low drag hull will give this factor a large value and permit the achievement of higher speeds through the water. Some values of (η_P/C_D) for amphibians are given in Table 1.

In order to obtain a physical picture of the amount of variation obtained, these values of (η_P/C_D) are plotted against vehicle width in Fig. 3. It is curious to note that there is a definite trend to higher efficiency with the wider vehicles. We can advance no reason as to why this should be so; possibly, it is merely an accidental grouping of the relatively few data points. However, the possibility of an adverse interference effect between two tracks might be an explanation.

All the values of (η_P/C_D) are very low, of course; perhaps an order of magnitude less than could be obtained by placing greater emphasis on hydrodynamic characteristics. The low values seem to result from both terms in the factor of merit; the drag coefficient C_D is very high on these vehicles, and the propulsive efficiency is very low. Only the first of these aspects will be studied in this paper.

The Definition of Resistance

Hull resistance (or drag) is usually broken down into four separate components, although we should bear in mind that this division is somewhat arbitrary.

Total resistance = Skin friction which is caused by shearing of the fluid close to the vehicle's skin. It is quite small for bluff bodies and may be neglected.
+ Pressure drag or form drag, which is caused by the fluid's inability to slow down without losing energy.
+ Wave drag, which represents the energy spent in making waves in the free surface.
+ Air drag, which is the aerodynamic counterpart of the first two components and is negligibly small for the low speeds associated with blunt forms.

We shall now discuss briefly these individual components, confining our attention to the first three. Of these, pressure drag and wave drag are by far the most important. Skin friction is included only because it has been considered as a significant factor by some workers in the past.

Skin-Friction Drag

The drag due to skin friction is given by the equation

$$D_{SF} = C_f \tfrac{1}{2}\rho u_s^2 A_{\text{wet}} \tag{10}$$

where C_f is the skin-friction drag coefficient, μ_s is the mean effective speed of the water over the wetted surface of the hull, and A_{wet} is the effective wetted area. For practical purposes there is no skin-friction contribution from the stern so that, from Fig. 1, the wetted area is

$$A_{\text{wet}} = \omega d + 2ld + \omega l \tag{11}$$

It is sufficient for present purposes to take $u_s = u$, the speed of the hull through the water. Also, we wish to express

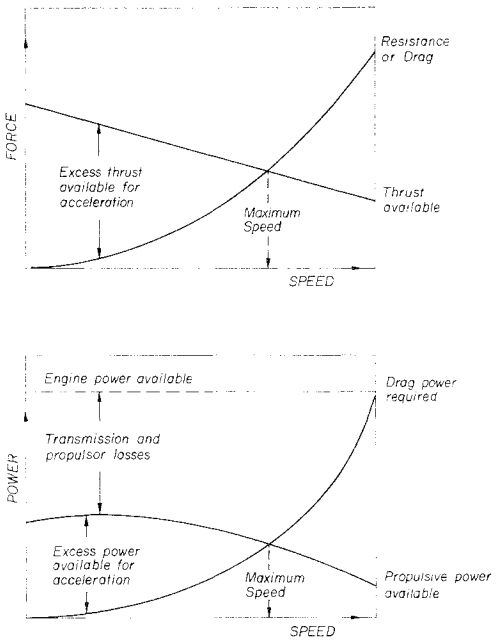

Fig. 2 Alternative presentations of power required and power available.

skin-friction drag as a coefficient based on the immersed frontal area, so that it will be directly comparable with estimates made for the other drag components. Thus, Eq. (10) becomes

$$\Delta C_{DSF} = C_f A_{wet}/A_F = C_f[1 + 2(l/\omega) + (l/d)] \tag{12}$$

For a typical amphibian (the LVTP-5, for example) $l/d = 8.06$ and $l/\omega = 2.54$. At its maximum speed of 6.8 mph, the Reynolds number is 2.4×10^7, corresponding to a skin-friction coefficient of $C_f = 0.0025$. Thus,

$$\Delta C_{DSF} = 14.1 C_f = 0.035$$

Since the total drag coefficient is typically of the order of unity, skin-friction drag in this case accounts for less than 4% of the total. This is considerably less than the figure of 10% sometimes quoted.

Pressure Drag

An ideal fluid of zero viscosity would flow past a body as shown in Fig. 4. Starting with an initial freestream velocity u_0, it speeds up to u_1 in the vicinity of the body and then slows down until it reaches the freestream value again. The process of accelerating and diffusing causes local energy

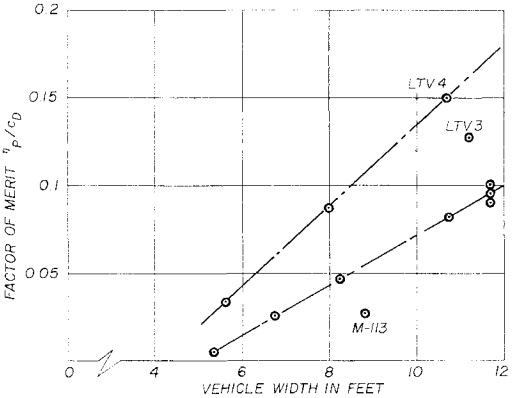

Fig. 3 Correlation of the factor of merit with vehicle width, for the amphibians listed in Table 1.

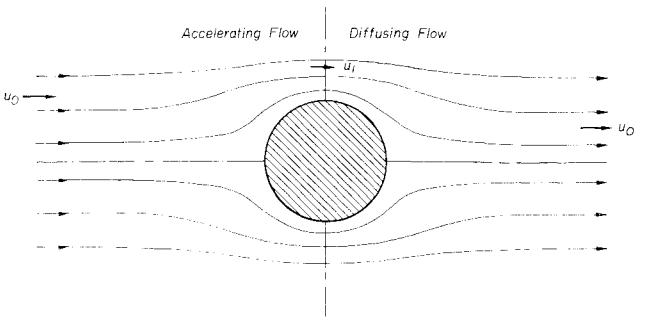

Fig. 4 Ideal (inviscid) fluid flow past a body.

changes (some of the pressure energy in the fluid is converted to kinetic energy in the vicinity of the body); but since this is a reversible process, there is no net loss of energy in the fluid and, therefore, no pressure drag force.

In a real (viscous) fluid, the situation is not so simple because of the boundary layer of slow moving fluid close to the surface of the body. As noted in the previous section, the direct drag contribution of this shear layer is small but it has a far-reaching effect upon the external flowfield that is not only not small but is, in fact, a dominating factor in bluff body drag.

When the flow is accelerating, as is the case to the left of station (1) in Fig. 4, the boundary layer is thin and stable, so that it has no appreciable effect upon the main body of the flow. Thus, the velocities and pressures are essentially those which would be measured in inviscid flow. Behind station (1) the fluid is slowing down, and this diffusion causes energy losses in the boundary layer and, eventually, separation from the surface. Thus, the fluid behind the body now has less energy than it has upstream, and this energy deficiency appears as a drag force acting on the body. That is,

$$\text{drag} \times \text{freestream velocity} = \text{loss in fluid energy}$$

Another way of describing the physical picture is sketched in Fig. 5. For inviscid flow the static pressure distribution over the body is symmetrical, so that the net force acting on it (the integral of the local pressure resultant) is zero. In a real fluid, the total pressure loss appears as a loss of static pressure over the rear portions of the body, so that the integral of this unsymmetrical pressure distribution gives a net drag force on the body.

It is, of course, generally true that the pressure drag arises from pressure differences around the body. The simple flow picture of the preceding paragraphs applies, however, only to the origins of pressure drag under full-scale conditions, that is, at high Reynolds numbers. At low speeds or for small models, or a combination of both, the flow picture can become much more complicated, as shown in Fig. 6, for the simple

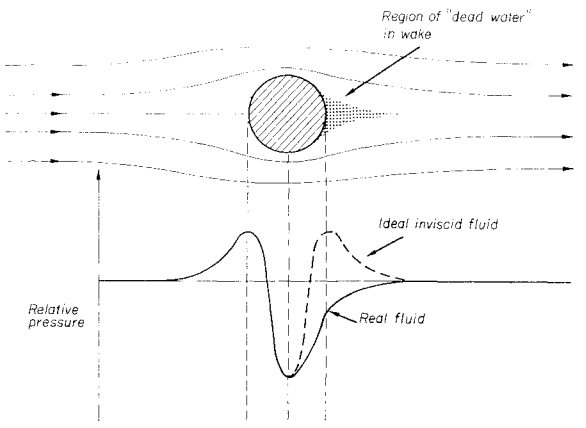

Fig. 5 Local static pressure distribution for a circular cylinder.

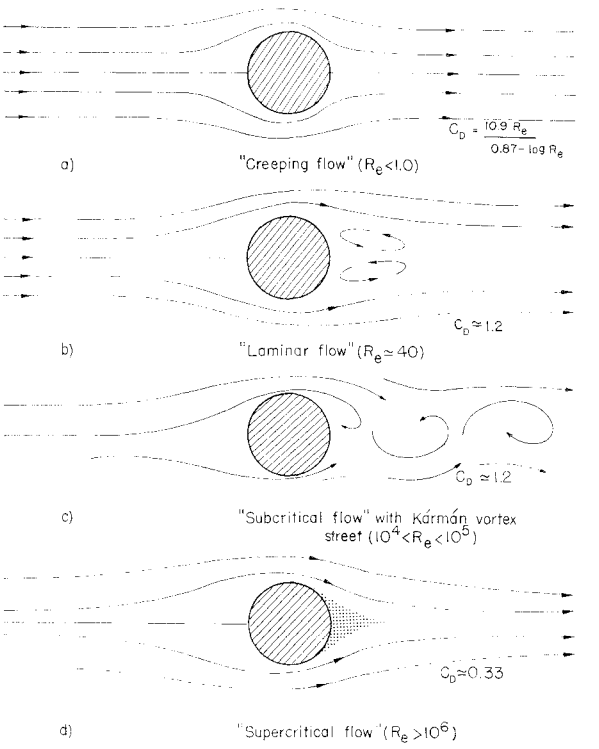

Fig. 6 Flow regimes experienced by a circular cylinder.

case of a circular cylinder. It is fortunate that the dimensions of full-size craft, coupled with the low kinematic viscosity of water, result in the major flow patterns always being supercritical. At low speeds or for small models, or a combination of both, the flow picture can become much more complicated, as shown in Fig. 6, for the simple case of a circular cylinder. It is fortunate that the dimensions of full-size craft, coupled with the low kinematic viscosity of water, result in the major flow patterns always being supercritical.

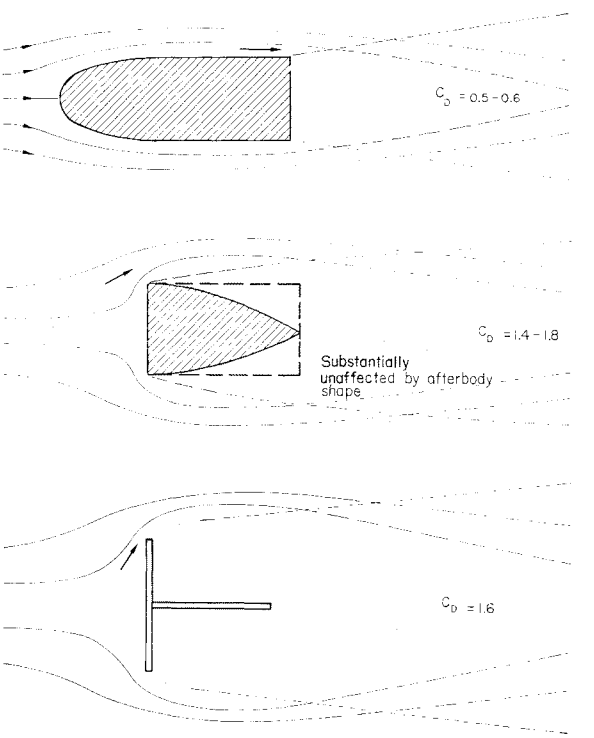

Fig. 7 Wake generation of various shapes.

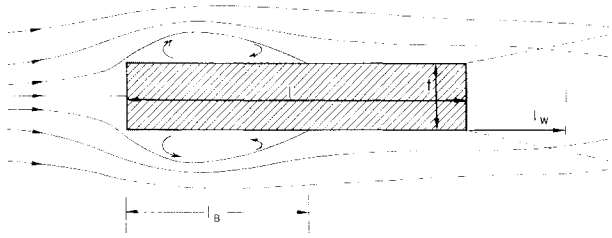

Fig. 8 Separation pattern over a lengthy bluff body.

Form (or Pressure) Drag Coefficient for Rectangular Shapes

Remembering that the high Reynolds number associated with full-scale hulls results in supercritical flow, some typical flow patterns around two-dimensional bluff bodies are sketched in Fig. 7. The most obvious feature is the wake behind the body, and it can be seen that, for sharp-edged bodies, these wakes fall into two general classes. If the forebody is streamline, so that the flow off the base region is parallel to the freestream, then the initial size of the wake is quite well defined by the width of the body. If the body has sharp corners at the front, however, the wake is much deeper, and the drag is rather more than twice that of the previous example. Finally, there is an intermediate case, as shown in Fig. 8, where the body has sharp corners at both ends but is long enough for the initially separated flow to reattach before reaching the stern.

Hoerner[3] presents data which show that, in two-dimensional flow, reattachment occurs if $l/t = 4.0$, and the nose separation bubble then contributes an apparent drag increment of approximately $\Delta C_D = 0.4$, as shown in Fig. 9. This increment should not be regarded as the actual drag caused by the separation bubble, however, but only as part of it. It can be shown that base drag depends mainly on the condition of the boundary layer immediately upstream of the base, and can be correlated by Hoerners[3] coefficient

$$C_{FS} = D_{\text{fore}}/q_0 A_S$$

where D_{fore} is the drag of the body portions upstream of the stern, q_0 is the freestream dynamic head, and A_S is the area of the stern. Thus, if C_{DB} is the bow drag coefficient,

$$C_{FS} = C_{DB}\, A_B/A_S$$
$$= C_{DB} \text{ for a rectangular cylinder}$$

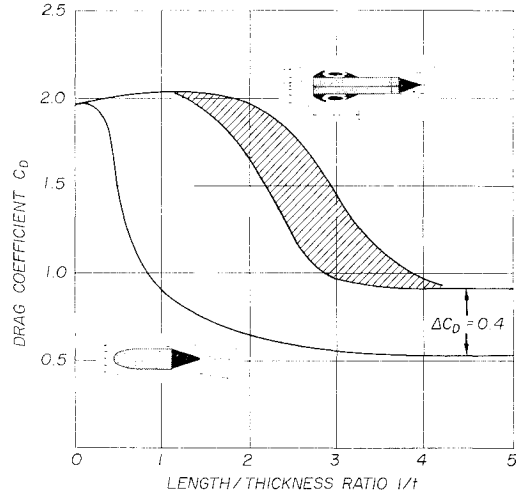

Fig. 9 Hoerner's[3] correlation of rectangular cylinder drag data.

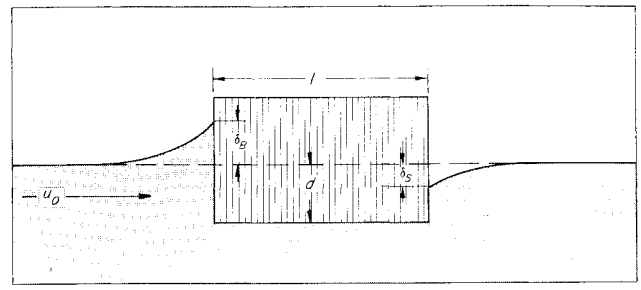

Fig. 10 Basic geometry for calculating wave drag.

Then from Hoerner's base drag correlation Ref. 3, pp. 3–20 we can show that

$$\left.\begin{matrix} C_{DB} \doteq 0.74 \\ C_{DS} \doteq 0.18 \end{matrix}\right\} (4.0 < l/t) \qquad \therefore C_D = 0.92$$

where C_{DS} is the coefficient of the stern drag contribution. It is of interest to note that the result $C_{DB} = 0.74$ can also be calculated by using "fluid friction" theory such as that described in Ref. 4.

As will be shown later, the two-dimensional value of $C_D = 0.92$ for $l/t = 4.0$ is in good agreement with Hay's[2] value of 0.9 for a box-like hull with $l/\omega = 4.0$. It therefore seems that three-dimensional effects on form drag may be small, at least when the body has sharp edges and the bow separation has reattached. On the other hand, there is reason for believing that reattachment may occur at lower values of l/t than 4.0 under three-dimensional flow conditions. (For example, compare Figs. 21 and 22, Ref. 3, pp. 3–12.) It should also be mentioned here that (unpublished) measurements of the bow drag of a rectangular cylinder in the Payne Inc. two-dimensional wind tunnel have given the result $C_{DB} = 0.72$.

Wave Drag Theory for Blunt Forms

Consider the blunt form shown diagramatically in Fig. 10. The total hull drag is partly caused by a pressure increase on the bow and partly by a reduction over the stern. What-

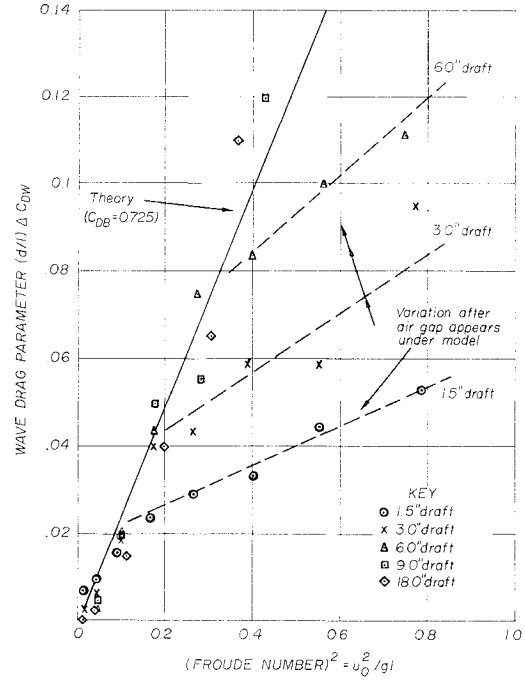

Fig. 11 Correlation of Hay's[2] data for the wave drag of a 36-in.-long model.

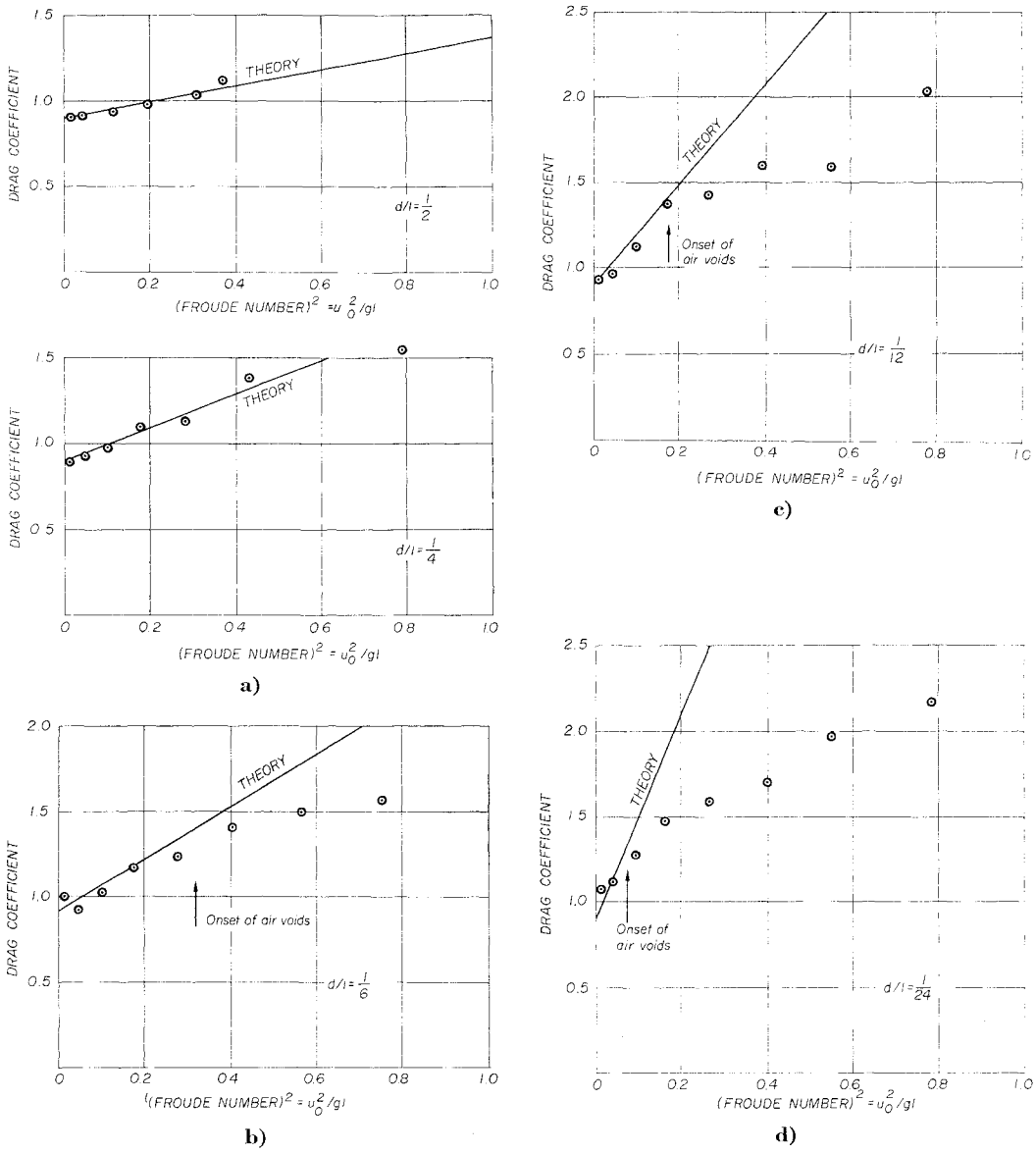

Fig. 12 Comparison of wave drag theory with experiment.

ever the pressure distribution along the parallel sides, it cannot influence the resultant drag force on the hull, of course. The total drag force on the bow must equal the average pressure rise (Δp_B) times the frontal area (A_F). If C_{DB} is the drag coefficient of the bow, based on the statically immersed frontal area, the bow drag force is

$$D_B = C_{DB}\tfrac{1}{2}\rho u^2 A_F = \Delta p_B A_F \qquad \therefore \Delta p_B = C_{DB}\tfrac{1}{2}\rho u^2 \quad (13)$$

We assume that the mean water level at the bow will rise to a height corresponding to this pressure, that is,

$$\delta_B = \Delta p/\rho g = C_{DB}u^2/2g \quad (14)$$

In the same way, the water level at the stern falls by an amount

$$\delta_S = C_{DS}\,u^2/2g \quad (15)$$

Thus, the total resultant drag is

$$D_T = D_B[1 + (\delta_B/d)] + D_S[1 - (\delta_s/d)] \quad (16)$$

In coefficient form,

$$C_D = (C_{DB} + C_{DS}) + C_{DB}(\delta_B/d) - C_{DS}(\delta_S/d)$$

But

$$\frac{\delta_B}{d} = \frac{C_{DB}u^2}{2gd} = \frac{C_{DB}F_l^2}{2(d/l)} \qquad \frac{\delta_S}{d} = \frac{C_{DS}u^2}{2gd} = \frac{C_{DS}F_l^2}{2(d/l)}$$

where F_l is the Froude number $\mu/(gl)^{1/2}$. Thus, the total drag coefficient, based on the statically immersed frontal area, is given by

$$C_{DT} = (C_{DB} + C_{DS}) + \frac{F_l^2}{2(d/l)}[C_{DB}^2 - C_{DS}^2] \quad (17)$$

= pressure drag coefficient + wave drag coefficient

Note that, in this case, the wave drag coefficient increases as the square of the Froude Number rather than as the fourth power associated with streamline forms.

Comparison with Experiment

A feature in Hay's[2] tests was the observed development of an air void at some critical speed, which was proportional in some way to the statically immersed depth of the model.

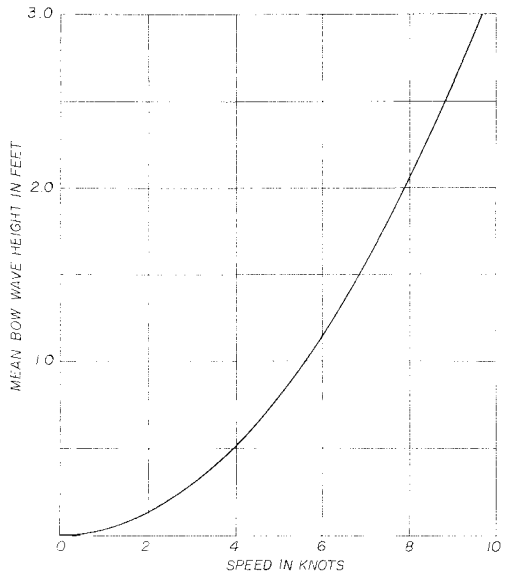

Fig. 13 Predicted variation of mean bow wave height with speed ($C_{DB} = 0.725$).

We naturally cannot expect the proposed wave drag theory to apply above this critical speed.

We can determine the total pressure drag coefficient ($C_D = C_{DB} + C_{DS}$) appropriate to Hay's model by plotting his drag coefficient data against the square of the Froude Number. It is obvious from Eq. (17) that we should then obtain a series of straight lines (below the void onset Froude Number) and that the intercept at $F_l = 0$ will give the pressure drag coefficient.

When this is done we obtain the result

$$C_D = (C_{DB} + C_{DS}) = 0.9$$

a value already deduced by Hoerner[3] from Hay's data, using another method of analysis. This is also in excellent agreement with the two-dimensional flow value given by Fig. 9, of course.

Subtracting this value of $C_D = 0.9$ from the measured total drag coefficient, we obtain the wave drag coefficient ΔC_{DW}. From Eq. (17) the product $(d/l)\Delta C_{DW}$ should be independent of immersion depth, so this product is used to correlate Hay's data in Fig. 11. When no void exists, the data are scattered about the theoretical line obtained by assuming $C_{DB} = 0.725$, $C_{DS} = 0.175$. These values are in excellent agreement with the values obtained in the preceding section. Although the scatter in Fig. 11 is relatively large, as seems always to be the case with this type of measurement, the agreement with the theory seems to be quite adequate up to the formation of the void. The theory is also compared with experiment in Fig. 12, using a different plot for each immersion depth in order to obtain greater clarity of presentation. The agreement here seems good enough to justify use of the theory for engineering purposes.

Discussion

The simple theory of this paper predicts that the water will "pile up" in front of a blunt form, to a mean "bow wave" height of

$$\delta_B = C_{DB}\, u^2/2g \qquad (18)$$

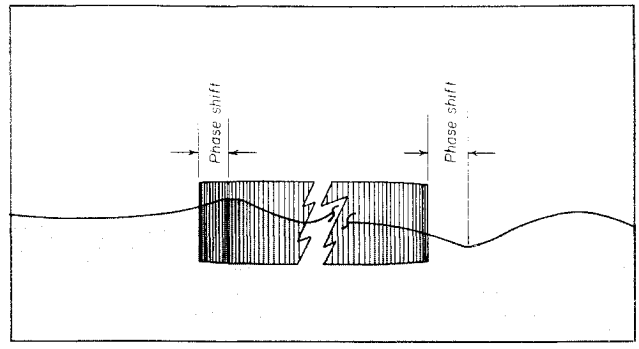

Fig. 14 The phase shift effect with a partially streamline hull.

which is plotted in Fig. 13. It is this increase in the effective immersed frontal area which is primarily responsible for the increase in drag with Froude number, although the reduction in immersed area at the stern also makes a small contribution.

It should be noted that Hay[2] implied this when he calculated his drag coefficients in terms of the observed frontally projected wetted area and showed that this caused all data points to fall on one line, at speeds below that at which an air void formed. In this present paper, we have been able to calculate this effect from first principles without the need to introduce experimentally determined constants in the usual sense. Thus, we may feel reasonably confident that the physical picture hypothesized is reasonably in accordance with what actually happens. Hoerner[3] also gives drag data for a barge shape with crudely streamlined bow and stern. In this case we find that the wave drag varies as the fourth power of the Froude number, rather than the square, so that the present theory will obviously not apply.

In the case of a rectangular form the water is constrained to pile up at the bow; also its level along the sides has no influence on the hull drag. When the bow is streamlined, however, and moving with an appreciable speed, the inertia of the water presumably causes a lag in its motion, as indicated in Fig. 14. Thus, its maximum elevation is somewhat behind the point of maximum pressure, and the idea that the mean water surface elevation is directly proportional to the local mean static pressure breaks down.

We would expect the blunt form theory to apply to a rectangular form whose edges were radiused, provided an appropriately lower drag coefficient value were used. Yet it does not apply when this edge radius is large enough to constitute a conventional bluff bow. It would obviously be interesting to see just where the dividing line lies and to obtain a clearer physical picture of the flow changes in this intermediate regime.

References

[1] Ingersoll, "Research, investigation and experimentation in the field of amphibian vehicles for the United States Marine Corps," Ingersoll Kalamazoo Div. of Borg Warner Corp. Final Report, Contract NOm 66245 (December 1957).

[2] Hay, A. D., "New coordinates for curves of resistance versus speed of blunt and semi-submerged forms," *The Marine Engineer and Naval Architect* (August 1950), p. 339.

[3] Hoerner, S. F., *Fluid Dynamic Drag* (Hoerner, S. F., Midland Park, N. J., 1958).

[4] Payne, P. R., "Viscous mixing phenomena with particular reference to thrust augmentors," AIAA Paper 64-798 (October 1964).